International Atomic Energy Agency

INDC(CPR)-026
Distr.: G

INDC INTERNATIONAL NUCLEAR DATA COMMITTEE

SEVERAL STUDIES ON MEDIUM ENERGY NUCLEAR DATA CALCULATION AND EVALUATION

Qing-biao Shen
Institute of Atomic Energy
Beijing, China

October 1992

IAEA NUCLEAR DATA SECTION, WAGRAMERSTRASSE 5, A-1400 VIENNA

INDC(CPR)-026
Distr.: G

SEVERAL STUDIES ON MEDIUM ENERGY NUCLEAR DATA CALCULATION AND EVALUATION

Qing-biao Shen
Institute of Atomic Energy
Beijing, China

October 1992

SEVERAL STUDIES ON MEDIUM ENERGY NUCLEAR DATA CALCULATION AND EVALUATION

Qing-biao SHEN
Institute of Atomic Energy, Beijing, China

Abstract

Several studies on medium energy nuclear data calculation and evaluation have been done in our institute recently. The subjects are: 1. Calculation of 5–50 MeV neutron induced reaction data of ^{56}Fe; 2. The study of neutron emissions at 585 MeV protons on ^{56}Fe with QMD; 3. Neutron relativistic phenomenological and microscopic optical potentials; and 4. Systematics of medium energy proton nonelastic and neutron total cross sections.

I. Introduction

Nowadays, more and more attention is being paid to the calculation and evaluation of medium energy nuclear data. Generally speaking, the projectile energy for medium energy nuclear data is 20–1000 MeV.

When the projectile energy is 20–50 MeV, although the number of the multi-particle emission channels is obviously larger than that below 20 MeV, the calculations for various multi-particle emission channels are possible and significant. Of course, the particle emission data and yield cross sections are also needed for calculation in this energy region. The conventional nuclear reaction theories such as optical model, Hauser-Feshbach theory, preequilibrum emission theory, evaporation model, and direct reaction theories, which are used very widely in the region below 20 MeV, may still be used. Some calculated results for 5–50 MeV neutron induced reactions of ^{56}Fe are presented in this paper.

When the projectile energy is larger than 40–50 MeV and less than 100–150 MeV, the non-relativistic approximation is still right. After making certain development and simplification, above mentioned theories may be used also in this energy region. The codes ALICE[1,2] and GNASH[3,4] are suitable to this energy region. Because there exist too many multi-particle emission channels, the calculation for various multi-particle emission channels is not necessary. The particle emission data and the yield cross sections are needed for the calculations only.

When the projectile energy is larger than 100–150 MeV, using above men-

tioned theories is not suitable. The intranuclear cascade models are generally used to describe the medium energy nuclear reaction processes[5,6]. In recent years, the quantum molecular dynamics (QMD) model has been developed[7,8], which is a very promising approach to be used in medium energy nuclear data calculation and evaluation. In this paper, the study of neutron emissions from 585 MeV protons interacting with ^{56}Fe with QMD finished by my coworkers will be briefly introduced[9]. When the incident nucleon energy is larger than 380 MeV, the pion production process should be considered[10].

The relativistic optical model is a powerful theoretical tool to calculate medium energy nucleon elastic scattering data. In this paper, a global neutron relativistic phenomenological optical potential obtained by us and some results of calculations using relativistic phenomenological and microscopic optical potentials are presented[11,12].

For those kinds of nuclear data, for which there exist plenty of experimental data, systematics may be used to obtain an empirical formula. Based on the systematic formulae by Letaw et al. and Pearlstein and considering as many experimental data as possible, new systematic formulae for medium energy proton nonelastic and neutron total cross sections are obtained [13], for which a brief introduction will presented here.

II. Calculation of 5–50 MeV Neutron Induced Reaction Data of ^{56}Fe

First, we made the program APNOM, by which the best neutron optical potential parameters in fitting experimental total and nonelastic cross sections and elastic scattering angular distribution data can be searched automatically. Second, we finished the program CMUP2 for charged particle or neutron

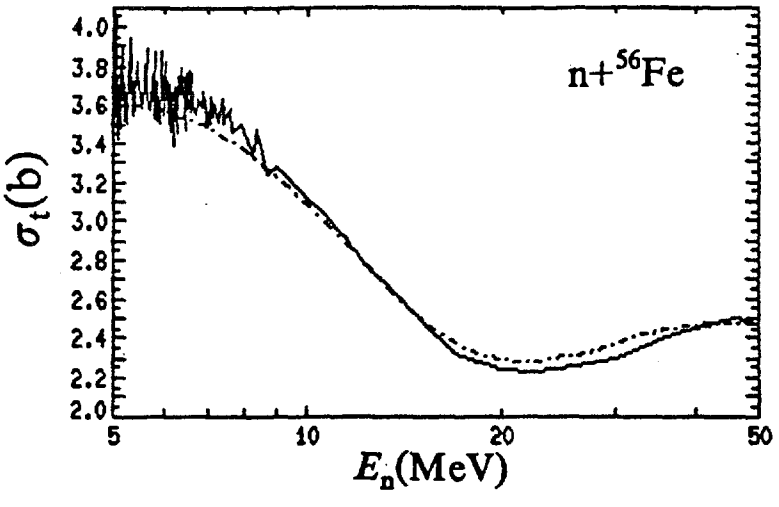

Fig. 1 Comparison of the calculated 5–50 MeV neutron total cross sections (dot–dash line) of ^{56}Fe with the evaluated values (solid line).

induced reactions for medium–heavy nuclei in the incident energy range up to 50 MeV based on the optical model, evaporation model and preequilibrium emission theory. The preequilibrium mechanism is applied in the first, second, and third emission processes. The pick–up mechanism in the first, second, and third composite particle formation during formation of equilibration and the Pauli principle in the calculation of exciton state densities are considered. The calculated direct reaction and compound elastic scattering results obtained with other codes can be added to the input data of the program CMUP2.

We collected various experimental data for the interaction of 5–50 MeV neutrons with ^{56}Fe, then, using the program APNOM, a set of best optical potential parameters is obtained as follows:

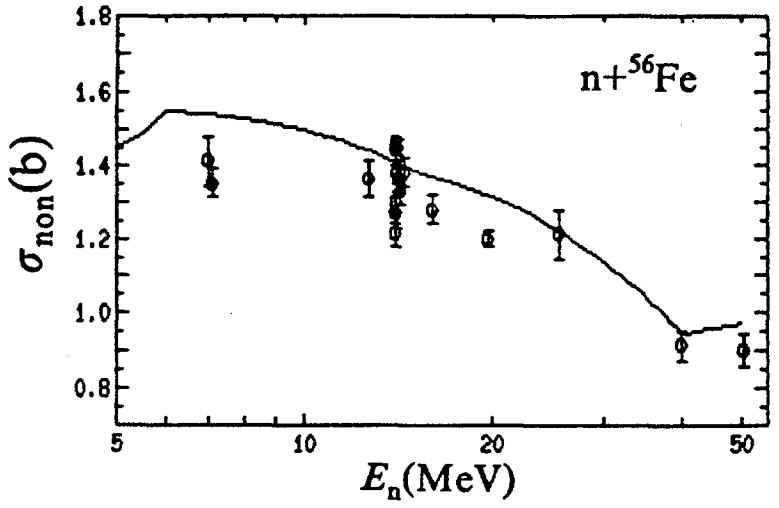

Fig. 2 Comparison of the calculated 5–50 MeV neutron nonelastic cross sections of ^{56}Fe with the experimental data.

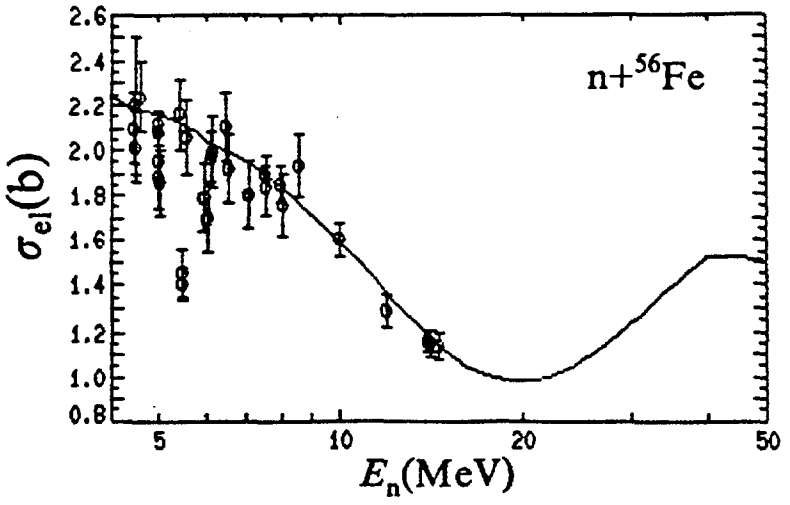

Fig. 3 The same as Fig. 2 except for elastic scattering cross sections.

$$V = 54.3759 - 0.48634E + 0.003575E^2 - 24.0(N-Z)/A, \quad (1)$$

$$W_s = 11.5977 - 0.26697E - 12.0(N-Z)/A,$$

or zero, whichever is greater, (2)

$$W_v = -0.89256 + 0.15548E - 0.00007E^2,$$

or zero, whichever is greater, (3)

$$r_r = 1.1939, \quad r_s = 1.3659, \quad r_v = 1.4828, \quad r_{so} = 1.1939 \quad (4)$$

$$a_r = 0.62462, \quad a_s = 0.48624, \quad a_v = 0.36001, \quad a_{so} = 0.62462 \quad (5)$$

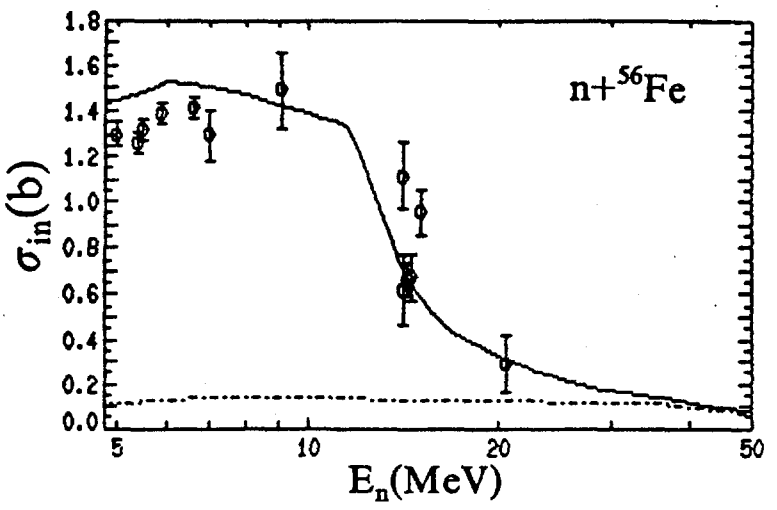

Fig. 4 Comparison of the calculated 5–50 MeV neutron inelastic scattering cross sections (solid line) of ^{56}Fe with the experimental data. The direct reaction contributions to the inelastic scattering cross section are presented by dot–dash line.

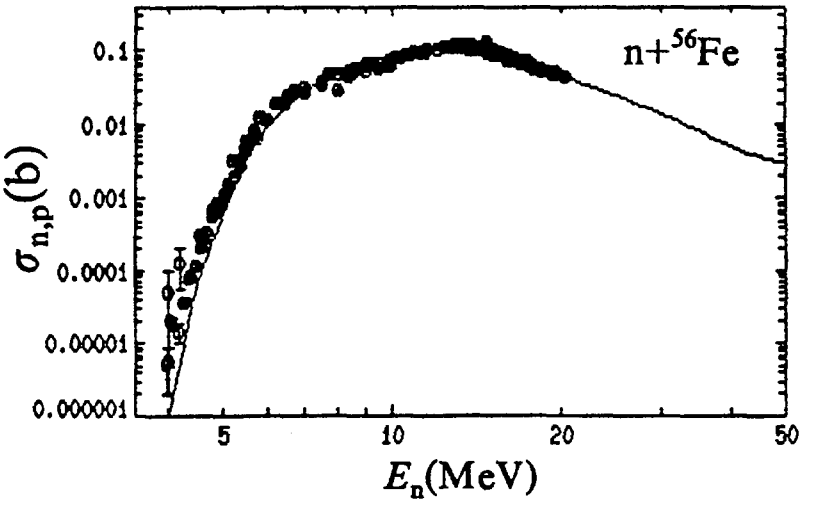

Fig. 5 The same as Fig. 2 but for (n,p) cross sections.

Using this set of neutron optical potential parameters and adjusting some charged particle optical potential and level density parameters as well as assuming the exiton model constant K = 300 MeV^3, the calculated results by the program CMUP2 are in good agreement with the experimental data taken from EXFOR and BNL-325[14].

Fig. 1 shows the comparison of 5–50 MeV neutron total cross sections of ^{56}Fe between the theoretical values (dot–dash line) and the evaluated values (solid line) taken from ENDF / B–6 for energies below 20 MeV and an eye guide curve for 20–50 MeV[14]. The calculated results are in good agreement with the experimental data. Fig. 2 shows the calculated 5–50 MeV neutron

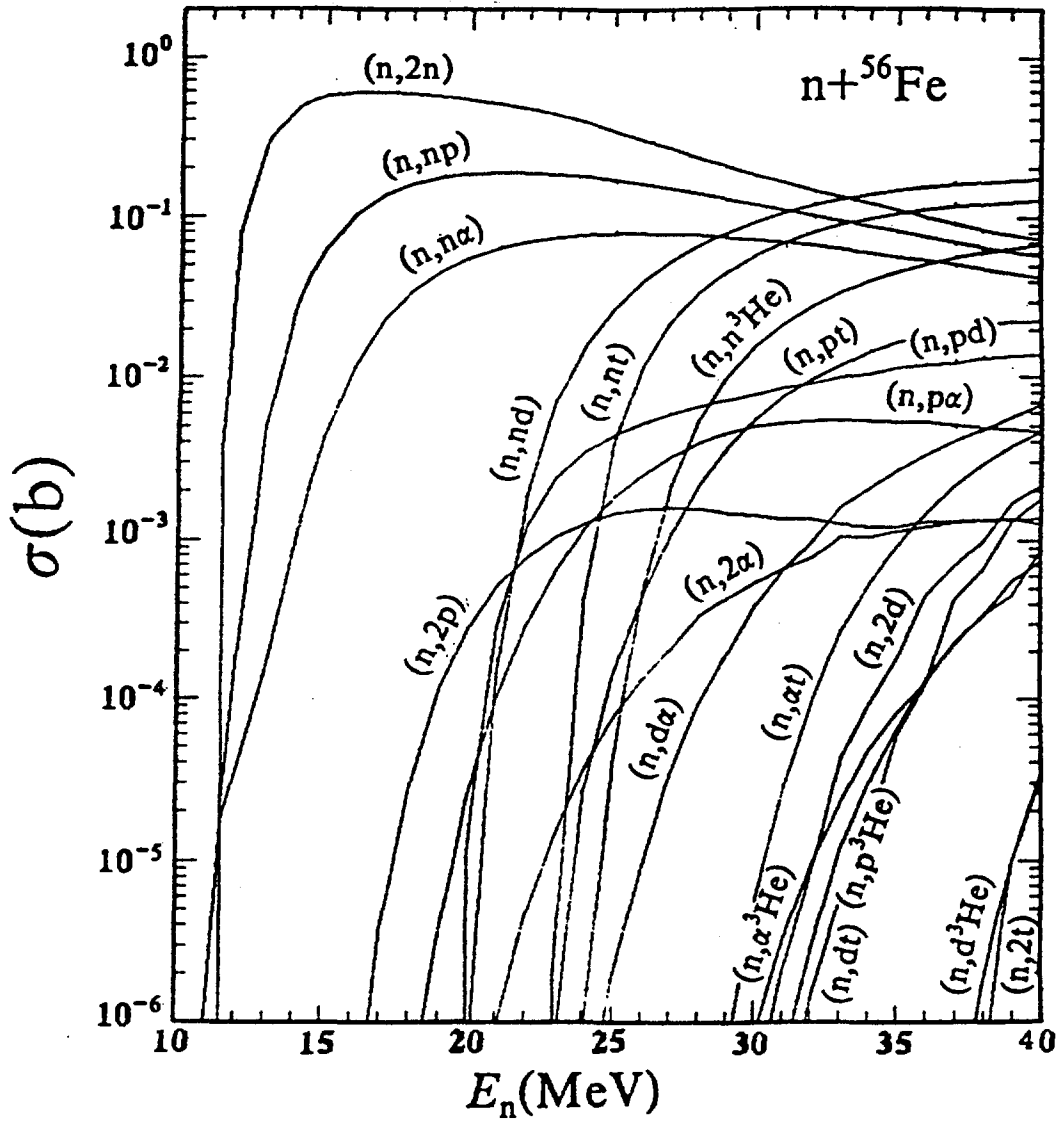

Fig. 6 The calculated neutron induced two–particle emission cross sections of ^{56}Fe below 40 MeV.

nonelastic cross sections. They are in reasonable agreement with the experimental data. Fig. 3 shows that the calculated elastic scattering cross sections agree with the experimental data pretty well. In Fig. 4 the calculated inelastic scattering cross sections (solid line) and the direct reaction contributions to the inelastic scattering cross sections (dot–dash line) are illustrated. The theoretical results are in reasonable agreement with the experimental data. One can clearly see that as the neutron energy is larger than 30 MeV the main contribution to the inelastic cross section comes from the direct reaction. Fig. 5 shows that the calculated (n,p) cross sections are in good agreement with the experimental data. Therefore, the calculated (n,p) cross sections in the 20–50 MeV

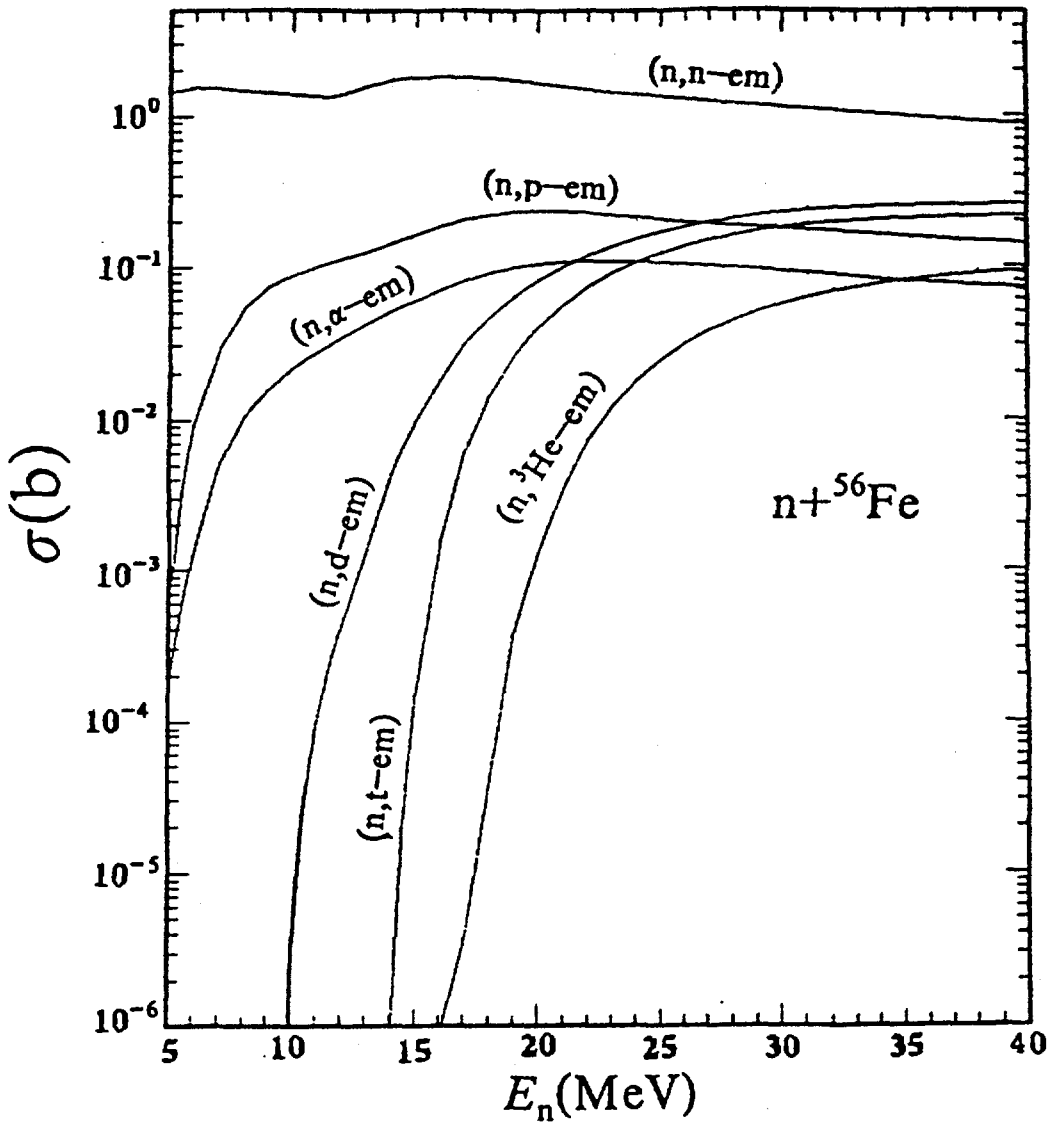

Fig. 7 The calculated neutron induced emission cross sections for 6 particles below 40 MeV.

region, for which there exist nearly no experimental data, are confident.

Fig. 6 illustrates various neutron induced two–particle emission cross sections below 40 MeV calculated by the program CMUP2. Evidently, the one–, three–, and four–particle emission processes must be considered simultaneously. It is clear that the multi–particle emission processes become very important in the 20–50 MeV region. Fig. 7 shows calculated neutron induced n–, p–, d–, t–, ^{3}He–, and α–emission cross sections below 40 MeV. Here the emission cross section means the sum of all the cross sections emitting the same particle. One can clearly see that the 5 kinds of charged particle emission cross sections are comparable and that t–em, d–em cross sections are larger

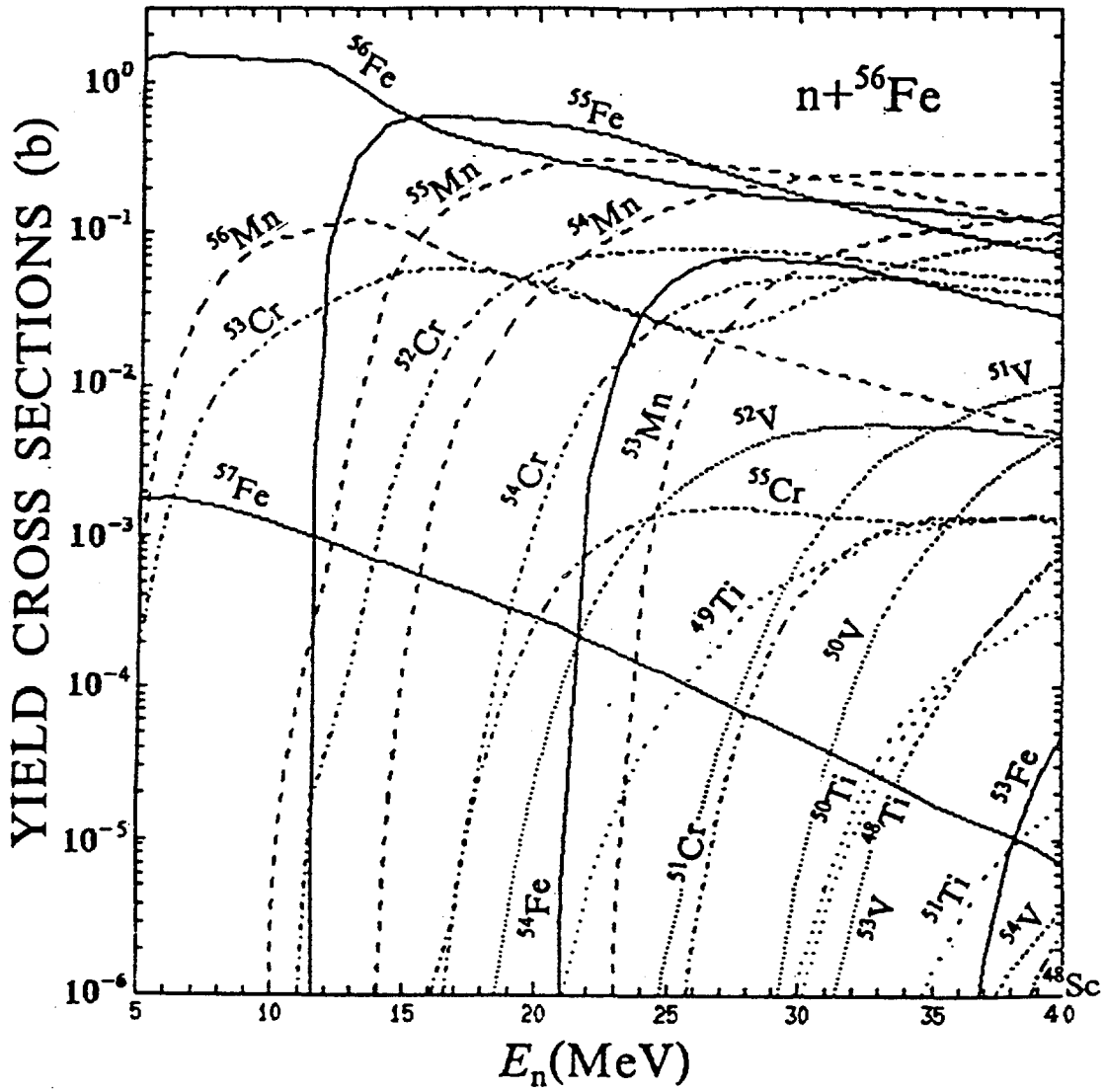

Fig. 8 The calculated yield cross sections in the reaction n+^{56}Fe below 40 MeV.

than the others in the 25–40 MeV region. Fig. 8 illustrates calculated neutron induced yield cross sections below 40 MeV. Many isotops of the elements Fe, Mn, Cr, V, Ti, and Sc can be produced in the reaction n+^{56}Fe. It is clear that the higher the nutron energy, the larger the number of yield nuclei.

Ⅲ. The Study of Neutron Emissions at 585 MeV Protons on ^{56}Fe with QMD

The analyses of medium energy nucleon–nucleus collisions are commonly based on the framework of the intranuclear cascade model. This model treats the reaction machanism in terms of a succession of nucleon–nucleon collisions with particles emitted at the various stages as the projectile energy is progressively dissipated in the target nuclei.

Newer approaches like VUU and QMD, in which a mean field is combined with an intranuclear cascade, are widely used in analysing heavy ion collisions. As a unified dynamical approach, it should also be valid when applied to nucleon–nucleus collisions.

Thus it is important to investigate the validity of QMD or VUU for the nucleon–nucleus collisions as a test of the capability of these microscopic dynamical approaches.

On the other hand, recently a unified approach for studying medium energy nuclear data has become highly necessary.

Motivated by these two aims, we study with QMD the particle emissions in the reaction of 585 MeV proton bombarding ^{56}Fe.

The Skyrme type density dependent force is used. But it should be pointed out that the expression of this part in Harmiltonian used in this work is $E_{dd.}=\frac{\alpha}{2}\frac{1}{\rho_0}<\rho>+\frac{\beta}{\gamma}\frac{1}{\rho_0^2}<\rho^{\gamma-1}>$, which is different from a original paper on QMD.

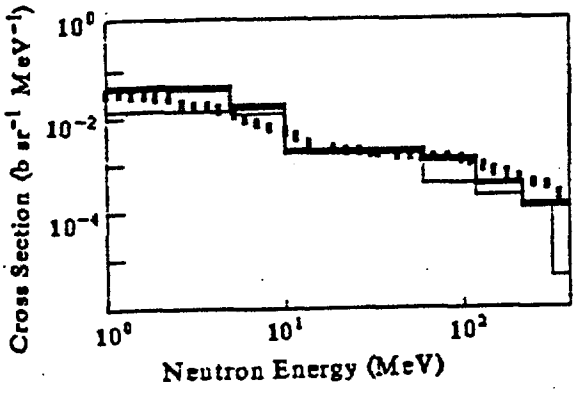

Fig. 9 Double differential cross sections of emitted neutrons at 30° lab. angle.

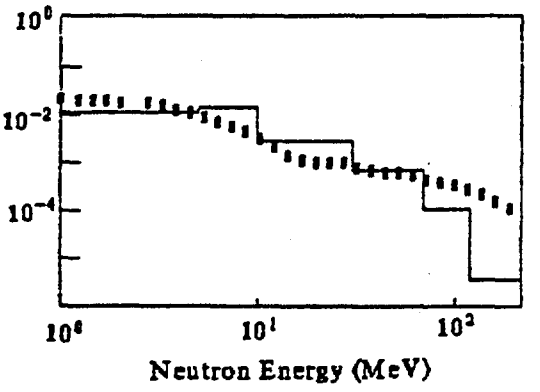

Fig. 10 Double differential cross sections of emitted neutrons at 90° lab. angle.

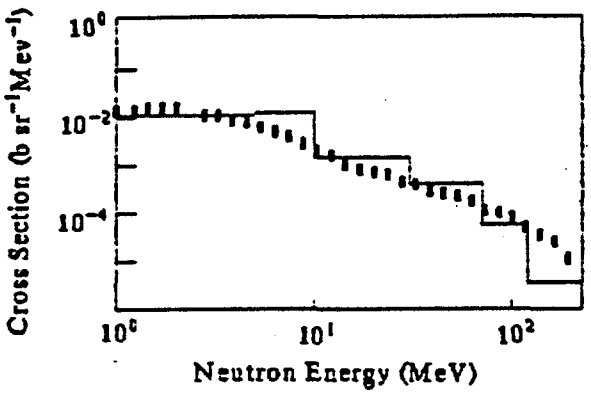

Fig. 11 Double differential cross sections of emitted neutrons at 150° lab. angle.

The stability of the initial target and its binding energy and rms radius are tested. The binding energy is about 8.8 ± 0.5Mev for all events. The rms radius is about 3.8 fm. The Fig.9 shows the comparison of calculated and measured [15] double differential cross sections of emitted neutrons at 30° laboratory angle. The thick line is for the hard equation of state (E.O.S.) and the thin one for the soft E.O.S. The agreement is quite good for both hard and soft momentum dependent E.O.S. Fig.10 and Fig.11 show the comparison of calculated and measured double differential cross sections of emitted neutrons at 90° and 150°, respectively. Generally, predictions of the QMD approach are in good agreement with measurement. The improvement in the cascade region is obvious compared to the intranuclear cascade–evaparation model[16]. Only the high energy tail part is still too low.

The particle emission mechanism and emission time are also studied. The preliminary results seem to be encouraging.

IV. Neutron Relativistic Phenomenological and Microscopic Optical Potential

In the medium energy domain, the nucleon relativistic optical model phenomenology based on the Dirac equation with a mixture of the Lorentz scalar potential and the time–like component of the Lorentz four–vector potential developed by Arnold and Clark[17,18] has been used to analyze the medium energy proton elastic scattering data with great success.

In the past, the form and parameters of the relativistic phenomenological optical potential (RPOP) have been extensively investigated. They were, however, restrictid to fit the experimental data for some specific target nuclei and in a certain range of incident energies. Only very recently global Dirac optical potentials for proton elastic scattering from heavy nuclei for energies between 65 and 1040 MeV have been published[19]. They are functions of both energy and target mass number. The number of parameters for set 1 and set 2 is 77 and 84, respectively.

The studies on neutron RPOP so far are rather limited due to the scarcity of experimental data. Recently more and more medium energy data have also become available. The availability of new neutron experimental data provides

the opportunity for studying the global neutron RPOP as well as its microscopic foundation.

In this paper, the global neutron relativistic phenomenological optical potentials for target nuclei ranging from ^{12}C to ^{238}U for incident energies $E_n = 20-1000$ MeV have been obtained through automatic search of the best-fit parameters by computer[11,12]. Then the relativistic nucleon-nucleus microscopic optical potential (RMOP) is studied with the effective Lagrangian based on the popular Walecka model including only nucleon, σ and ω meson with two adjustable isoscalar meson coupling constants g_σ and g_ω chosen to reproduce the nuclear matter saturation properties[20-22].

In relativistic optical model analyses of medium energy scattering experiments we use the Dirac equation. The Lorentz scalar potential U_S and the time-like component of a four-vector potential U_0 are assumed to be complex and dependent on energy and mass number of the target nuclei, and they can be treated either as a strictly phenomenological model with a number of adjustable parameters or as a microscopic model derived from some more basic theory without any free parameters. In the above mentioned two approaches, the Schrödinger equivalent central potential U_{eff} and spin-orbit potential U_{SO} can be obtained, simultaneously.

In the following part, we are aiming to obtain a global neutron relativistic optical potential, whose parameters are functions of both energy and target mass number. The experimental data used for this purpose consist of ten nuclei from ^{12}C to ^{238}U over a wide energy region from 20 up to 1000 MeV. The total cross section data taken from Refs.[14,23-25] are quite complete; they cover the whole energy range for all ten nuclei considered in this paper. The nonelastic cross section data available only below 200 MeV for some specific nuclei[14] and the elastic scattering angular distribution data for energies between 20 and 40 MeV for ^{12}C, ^{16}O, ^{27}Al, ^{56}Fe, ^{208}Pb and ^{209}Bi[26-31] as well as at 96 MeV for ^{12}C in the small angle region[32] and at 155 MeV for ^{12}C, ^{27}Al, ^{63}Cu, and ^{208}Pb also within the small angle range[33] are all neutron data accessible to us in addition to the rather complete set of total cross section. Our global neutron relativistic phenomenological optical potential is parameterized on the basis of above mentioned data set.

We choose scalar and vector optical potentials of the Woods-Saxon form, whose parameters depend on energy E, mass number A and charge number Z. Through automatic search of the best parameters in fitting the experimental data σ_t , σ_{non} and $\sigma_{el}(\theta)$ by computer, a global neutron RPOP, which contains 38 paramcters, has been constructed as follows:

$$U_0(r) = V_0 f_0(r) + iW_0 g(r), \tag{6}$$

$$U_S(r) = V_S f_S(r) + iW_S g(r), \tag{7}$$

$$V_0 = 304.08 - 0.1103E^{0.8451+0.000634A} - 0.0000922E^{1.968-0.000787A} - 2.295\alpha - 5.666\beta, \tag{8}$$

$$V_S = -379.66 - (0.05492 + 0.0000241A)E - 3.637\alpha + 13.328\beta, \tag{9}$$

$$W_0 = -5.090 - (0.2146 + 0.0000464A)E^{0.8945-0.000283A} + 0.00000562\beta E^2 + 23.692\alpha + 1.982\beta, \tag{10}$$

$$W_S = -14.21 + (0.2820 - 0.000395A)E^{0.8934-0.000285A} + 18.895\alpha - 1.189\beta \tag{11}$$

$$\alpha = \frac{N-Z}{A}, \qquad \beta = \left|\frac{A-64}{A+16}\right|^{1.278}, \tag{12}$$

$$f_i(r) = \left\{1 + exp\left[(r - r_i A^{\frac{1}{3}})/a_i\right]\right\}^{-1}, \qquad i = 0,\ s \tag{13}$$

$$g(r) = \left\{1 + exp\left[(r - r_W A^{\frac{1}{3}})/a_W\right]\right\}^{-1}, \tag{14}$$

$$r_0 = 1.164, \qquad r_S = 1.159, \qquad r_W = 1.239$$

$$a_0 = 0.5746, \qquad a_S = 0.5923, \qquad a_W = 0.4378$$

For the relativistic microscopic optical potential (RMOP), we adopted an approach to the relativistic many–body theory based on the effective Lagrangian density of the Walecka model, which allows to perform the calculations for the nucleon–nucleus interactions in the lowest order approximation. The merit of this approach is obviously that it is very simple, and can easily be applied to the scattering problem.

We start from an effective Lagrangian with two adjustable isoscalar meson coupling constants g_σ and g_ω. The values of the nucleon and ω meson masses are taken from the experiments, M = 938.9 MeV and M_ω = 783 MeV. The mass of the hypothetical σ meson is fixed to M_σ = 550 MeV, which is commonly used in the NN interaction to simulate the two π exchange.

In the next part, we are going to study the nucleon RMOP. It is known that the self–energy of a nucleon in the nuclear medium is identified with the effective interaction of the nucleon with the nuclear medium, i.e. nuclear optical potential. Based on the Feynman diagram rules one could perturbatively derive the nucleon self–energy in nuclear matter. We let only the second–order (Hartree–Fock) self–energy of a nucleon in the nuclear medium represent the

real part of the optical potential and consider the imaginary part of the fourth–order self–energy as the imaginary part of the optical potential.

The effective coupling constants g_σ and g_ω are adjusted by requiring that the empirical saturation properties of the nuclear matter are reproduced, i.e. the binding energy per nucleon $\varepsilon/\rho_B - M = -15.75$ MeV and pressure $P = 0$ at the normal density, corresponding to $k_F = 1.42$ fm^{-1}.

The calculations of the self–energy of a nucleon are first carried out in the nuclear matter up the fourth–order as mentioned above. The optical potential for finite nuclei is then obtained within the LDA. The density distribution is taken from Negele's empirical formulae[34], except for light nuclei such as ^{12}C and ^{16}O[35]. Thus we could obtain a RMOP without any free parameters.

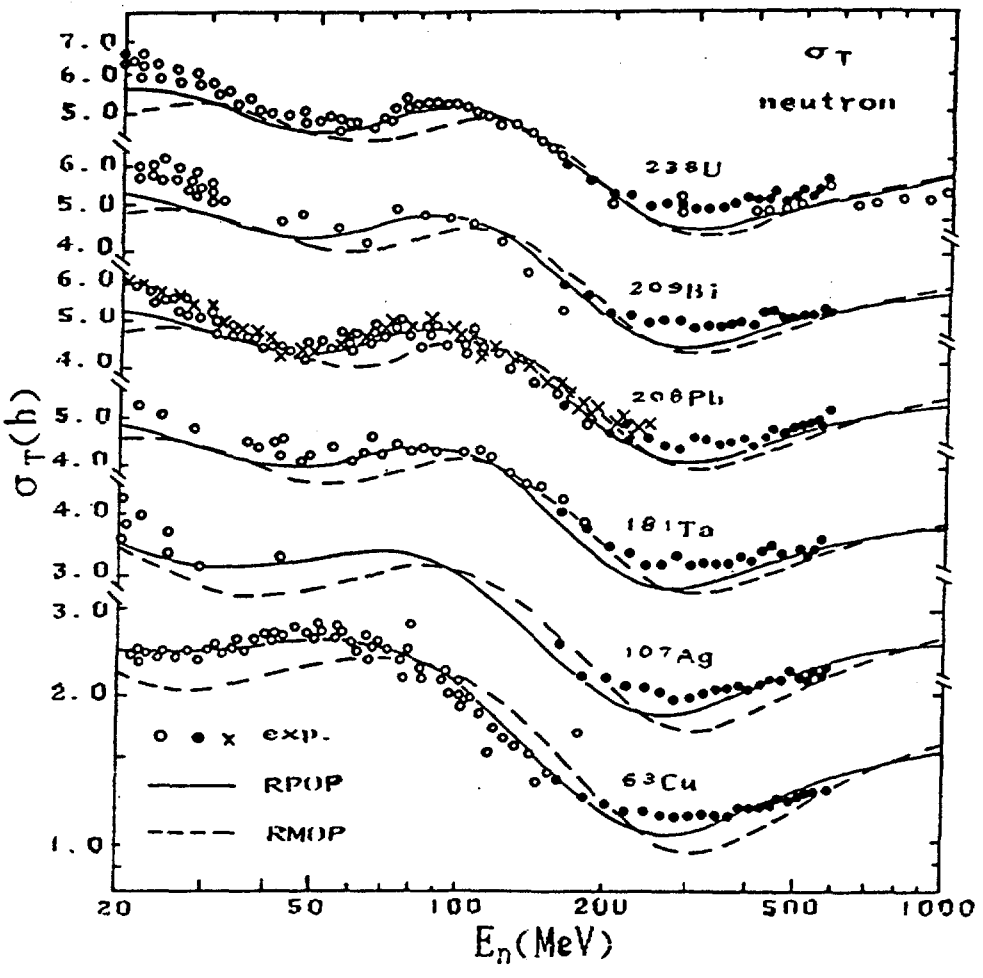

Fig. 12 Neutron total cross sections for ^{63}Cu, ^{107}Ag, ^{181}Ta, ^{208}Pb, ^{209}Bi, and ^{238}U at energies 20–1000 MeV calculated with RPOP (solid line) and RMOP (dashed line). The experimental data are taken from Refs.[14,23–25].

The real parts of the central Schrödinger equivalent potentials of neutron RPOP and RMOP for ^{56}Fe at various energies are calculated. For energies $E_n < 500$ MeV the real potentials of both RPOP and RMOP are rather close to each other and the so–called "bottom of wine bottle" shape is found in both of them in the 200–300 MeV energy region. For energies $E_n > 500$ MeV the V_{eff} of RMOP continues to go up rapidly as energy increases, while the one of RPOP first increases slowly with energyand then even comes down as energy goes up . The imaginary potentials always assume negative values. The values of the imaginary potentials of RMOP increase much more rapidly with energy as compared with those of RPOP. The spin–orbit Schrödinger equivalent potentials of neutron RPOP and RMOP in the same energy region are also calculated. One can see that the real spin–orbit potentials V_{SO} are negative

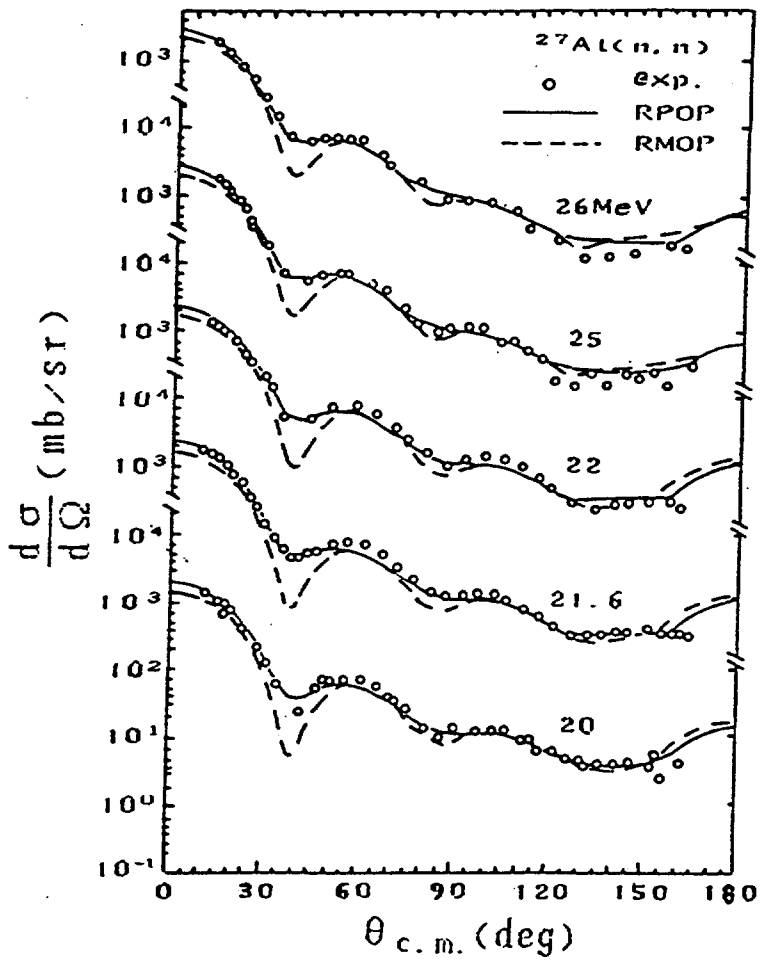

Fig. 13 Neutron elastic scattering angular distributions for ^{27}Al at energies 20, 21.6, 22, 25, and 26 MeV calculated with RPOP (solid line) and RMOP (dashed line). The experimental data are taken from Refs.[26,28].

whereas the imaginary ones W_{so} are positive. The absolute value of V_{so} decreases as energy increases , but that of W_{so} increases as energy increases. The imaginary part W_{so} can be neglected at low energies but both the real and imaginary spin–orbit potentials should be considered simultaneously at high energies.

The neutron total cross sections σ_t, nonelastic cross sections σ_{non} and elastic scattering angular distributions $\sigma_{el}(\theta)$ for ten target nuclei ranging from ^{12}C to ^{238}U with incident energies $E_n = 20–1000$ MeV have been calculated with both RPOP and RMOP.

Fig. 12 shows the comparison of neutron total cross sections for 6 target

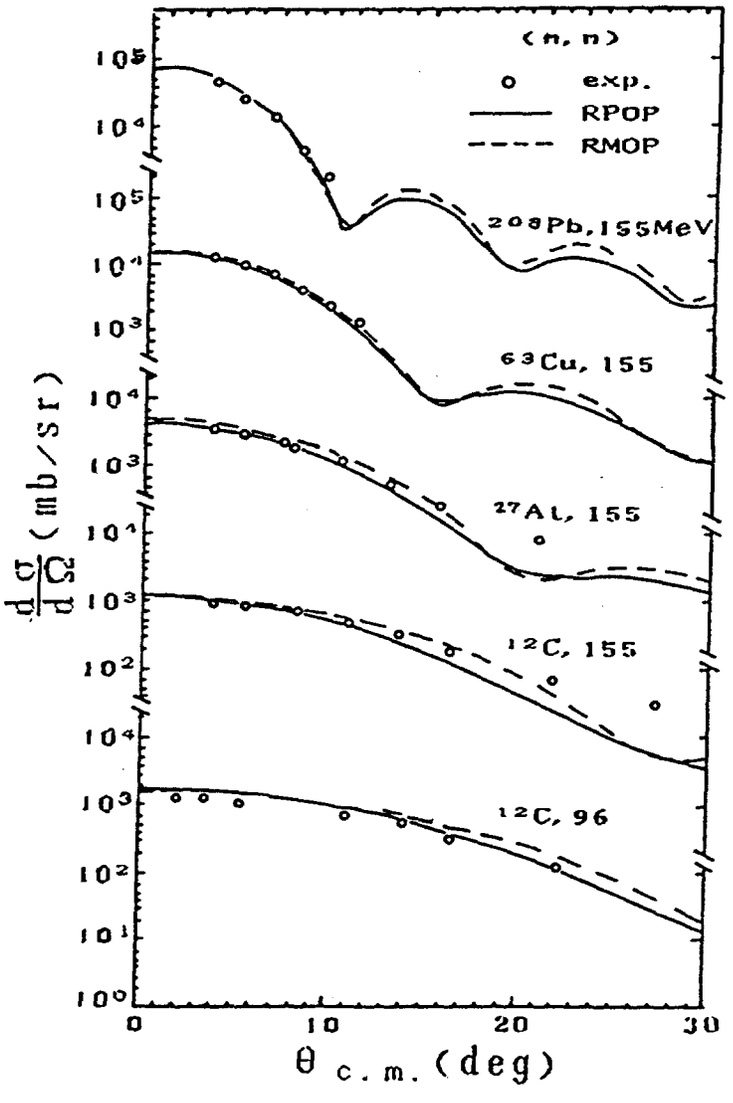

Fig. 14 The same as Fig. 13 except for ^{12}C at energy 96 MeV and for ^{12}C, ^{27}Al, ^{63}Cu, and ^{208}Pb at 155 MeV. The experimental data are taken from Refs.[32,33].

nuclei calculated with RPOP and RMOP with the experimental data. Generally speaking, the values and tendency of the total cross sections calculated by RMOP agree with the experiments pretty well and the results of RPOP are rather close to the experiments.

Fig.13 shows the neutron elastic scattering angular distributions for ^{27}Al in the energy region of 20–26 MeV calculated by RPOP and RMOP. The experimental data are taken from Refs[26,28]. For most cases the calculated results obtained with both RPOP and RMOP are in pretty good agreement with the experiments, but the valleys in the results by RMOP are too deep as compared with experiments. In Fig.14 the elastic scattering angular distributions for ^{12}C at 96 MeV and for ^{12}C, ^{27}Al, ^{63}Cu and ^{208}Pb at 155 MeV calculated by RPOP and RMOP are illustrated. The expermental data are taken from Refs.[32,33]. The overall good agreement with experiments for both RPOP and RMOP is seen except at some specific points.

V. Systematics of Medium Energy Proton Nonelastic and Neutron Total Cross Sections

The proton nonelastic or reaction and neutron total cross sections are the most important and basic. Nowadays, large amounts of experimental data for both of them have been accumulated. The experimental data of medium energy proton nonelastic cross sections were collected and published[36,37]. The experimental data of medium energy neutron total cross sections can be found in some references[14,23–25,38]. These two kinds of medium energy cross sections can be calculated with the relativistic optical model[19,12]. However, in order to fit the experimental data there are too many adjustable parameters in the relativistic optical model calculation for selection. Considering that there are many experimental data for these two kinds of cross sections, studying their systematics is obviously valuable in practice.

Based on the analysis of experimental data, Letaw obtained a systematic formula of proton nonelastic cross sections for energies higher than 20 MeV above the Coulomb barrier[39]. Then, based on the Letaw formula, Pearlstein obtained a systematic formula of the neutron total cross sections for energies above 20 MeV[2] and both formulae are used in the calculations of medium energy nuclear data for the reactions p+^{56}Fe and n+^{56}Fe[24,2]. In order to examine the Letaw medium energy proton nonelastic cross section systematic formula, we chose the following 12 nuclei: ^{12}C, ^{16}O, ^{27}Al, ^{40}Ca, ^{56}Fe, ^{63}Cu, ^{90}Zr, ^{107}Ag, ^{118}Sn, ^{181}Ta, ^{208}Pb, and ^{238}U, which have more experimental data. Through calculations and comparisons with experimental data, it is found that the calculated results using the Letaw medium energy proton σ_{ne} formula agree with the

experimental data pretty well for light nuclei, but become worse for $A \geqq 40$ heavier nuclei. Although for heavier nuclei the calculated results obtained with the Letaw formula agree with the experimental data still better in the $E > 100$ MeV high energy region, it becomes obviously far larger than experimental data in the low energy region, and the heavier the nuclei, the larger the deviation. Thus, the Letaw proton nonelastic cross section systematic formula is not universal. In order to examine the Pearlstein medium energy neutron total cross section systematic formula, we chose the following 10 nuclei: ^{12}C, ^{16}O, ^{27}Al, ^{56}Fe, ^{63}Cu, ^{107}Ag, ^{181}Ta, ^{208}Pb, ^{209}Bi, and ^{238}U, which have more experimental data.

The aim of this work is to improve the Letaw and Pearlstein systematic formulae. First, some changes on their systematic expressions are made. Then we define

$$X^2 = \frac{1}{M} \sum_{i=1}^{M} \frac{1}{N(i)} \sum_{j=1}^{N(i)} \left(\frac{\sigma_C(i,j) - \sigma_E(i,j)}{\Delta\sigma_E(i,j)} \right)^2 \tag{15}$$

where σ_C is the calculated cross section value, σ_E the experimental cross section value, and $\Delta\sigma_E$ expresses the experimental error. The sum over i and j denotes the sum over all chosen nuclei and energies, respectively. The parameters of the new systematic formula can be obtained through automatic computer search of the minimum deviation between the calculated results and the experimental data. After careful researching, the new medium energy proton nonelastic cross section systematic formula is obtained as follows:

$$\sigma_{ne}(A,E) = 0.0426A^{0.701} f(A)g(E)h(A,E) \tag{16}$$

$$f(A) = 1 + 0.0144Sin(3.63 - 2.82logA) \tag{17}$$

$$g(E) = 1 - 0.67e^{-E/150} Sin(12E^{-0.289}) \tag{18}$$

$$h(A,E) = [1 + (0.018A^2 - 1.15A)/E^2]^{-1} \tag{19}$$

The unit of the cross section is barn. Figs.15–17 show the comparisons of the proton nonelastic cross sections calculated with our new formula and with the Letaw formula with the experimental data for ^{12}C, ^{56}Fe, and ^{208}Pb. In these figures, besides the isotope experimental data also the corresponding natural element experimental data are given. It is seen that the calculated results obtained with our new formula for the 12 nuclei in the range $A = 12$–238 for energies E_p = few–1000 MeV are all in pretty good agreement with the experiments. Both the experimental data and calculated results show that the proton nonelastic cross sections have a broad peak at about several ten MeV and a minimum at about 200–300 MeV. The calculated results obtained with the

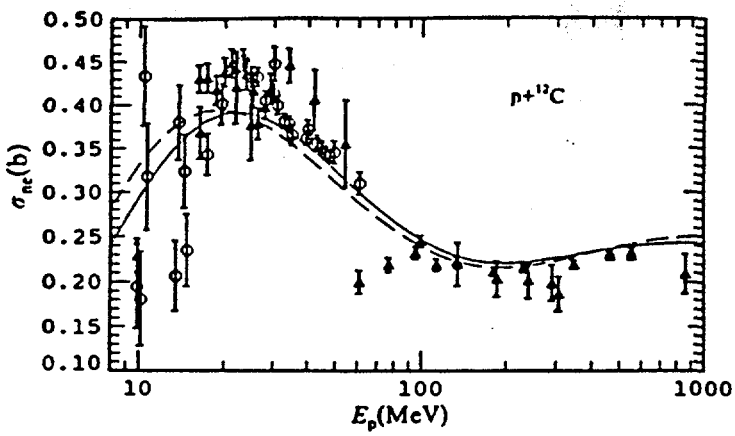

Fig.15 Comparison of the medium energy proton nonelastic cross sections calculated with the Letaw systematic formula (dashed line) and our systematic formula (solid line) with experimental data for ^{12}C[36]. The symbols circle and triangle represent the experimental data for isotope and corresponding natural element, respectively.

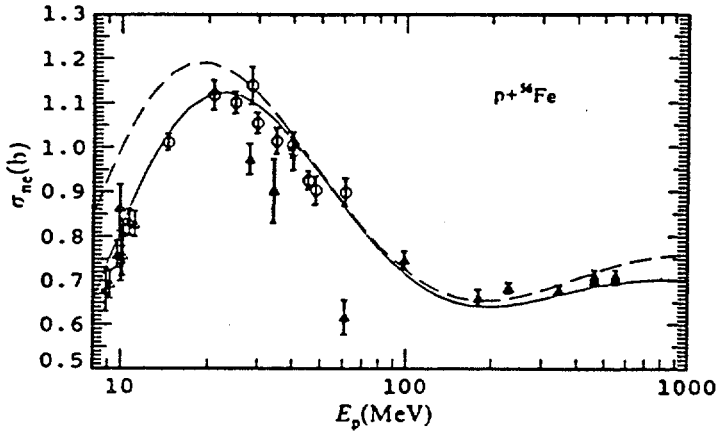

Fig.16 The same as Fig.15 except for ^{56}Fe and the experimental data taken from references [36] and [37].

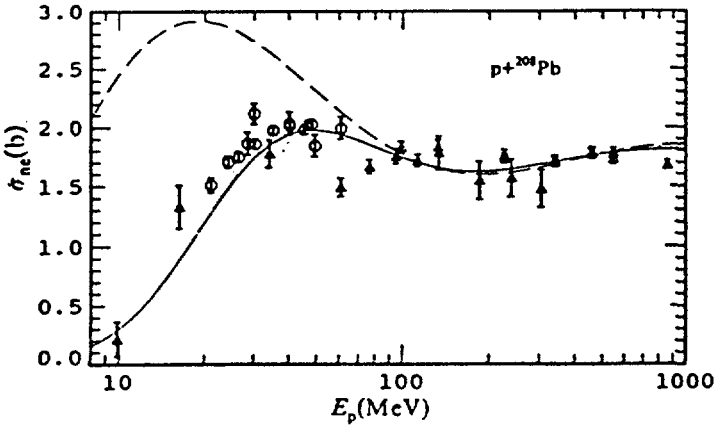

Fig.17 The same as Fig.15 except for ^{208}Pb.

Letaw proton nonelastic cross section formula become very bad for A≧40 heavier nuclei in the low energy region, but our new formula overcomes this drawback. So far, the proton nonelastic cross section experimental data are not sufficient and are scattered, therefore, the recommended systematic formula in this paper should be improved when more and better experimental data are available in the future.

By use of the same method, our new medium energy neutron total cross section systematic formula is as follows:

$$\sigma_t(A,E) = 0.04586A^{0.7}s(A)t(E)(1+k_4) + k_1A^{1/3}\sum_{i=1}^{2} e^{-[k_2 log(E_{pi}/E)]^2} \tag{20}$$

$$s(A) = 1 + 0.02946Sin(3.03 - 1.967logA) \tag{21}$$

$$t(E) = 1 - 0.57e^{-E/298}Sin(10.63E^{-0.2836}) \tag{22}$$

$$E_{p1} = k_3A^{1/3} \tag{23}$$

$$E_{p2} = E_{p1} - 13.78A^{1/3} + 0.275(51-A)\Theta(51-A) \tag{24}$$

$$logk_1 = 0.298 - 0.685logA + 0.075(logA)^2 \tag{25}$$

$$logk_2 = -0.297 - 0.0124logA + 0.0292(logA)^2 \tag{26}$$

$$logk_3 = 0.929 + 0.726logA - 0.0709(logA)^2 \tag{27}$$

$$logk_4 = -2.14 + 0.487logA - 0.0271(logA)^2 \tag{28}$$

$$\Theta(51-A) = \begin{cases} 0 & 51-A \leqq 0 \\ 1 & 51-A > 1 \end{cases} \tag{29}$$

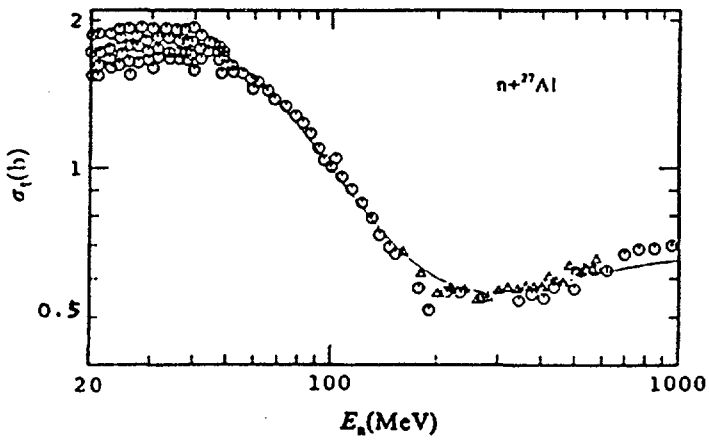

Fig.18 Comparison of the medium energy neutron total cross sections calculated with our new systematic formula (solid line) with experimental data for ^{27}Al. The symbols circle and triangle represent the experimental data taken from references[14,23,24,38], respectively.

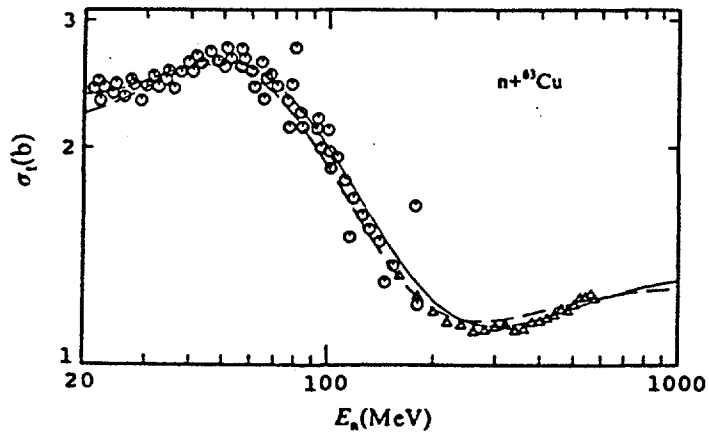

Fig.19 Comparison of the medium energy neutron total cross sections calculated with Pearlstein's systematic formula (dashed line) and our new systematic formula (solid line) with experimental data for ^{63}Cu. The symbols circle and triangle represent the experimental data taken from references[14,23,24,38].

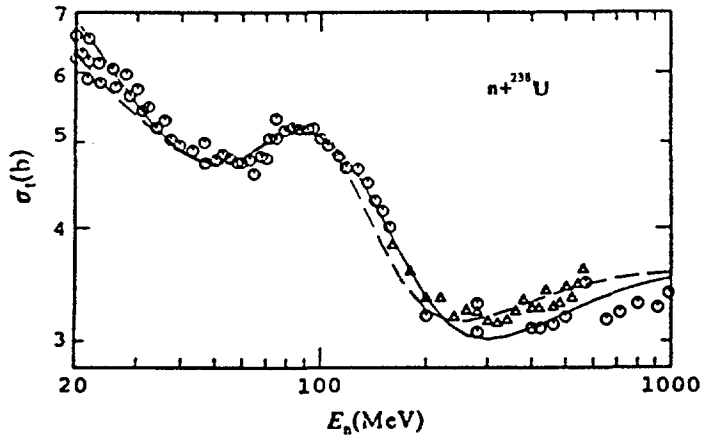

Fig.20 The same as Fig.19 except for ^{238}U.

The unit of the cross section is barn, too. Figs.18–20 show the comparison of the neutron total cross section calculated with our new formula and with Pearlstein's formula with experimental data for ^{27}Al, ^{63}Cu, and ^{238}U. It is seen that the calculated results obtained with our new formula for $E_n = 20–1000$ MeV for 10 nuclei in the range $A = 12–238$ are all in pretty good agreement with the experiments. It is also shown that the calculated results obtained with our new formula are better than those obtained with the Pearlstein formula. Of course, the medium energy neutron total cross section systematic formula obtained in this paper should be further developed when more experimental data become available.

VI. Summary

Based on the available experimental data, we obtained a set of 5–50 MeV neutron optical potential parameters for ^{56}Fe. Then adjusting some charged particle optical potential and level density parameters as well as taking the exiton model constant $K = 300\ MeV^3$, the various calculated nuclear data are all in better agreement with the experimental data in the above mentioned energy region. Therefore, the various predicted cross sections, yields, angular distributions, and emitted particle energy spetra in this energy region are reliable to some extent.

The particle emissions in the reactions of 585 MeV protons bombarding ^{56}Fe were studied with QMD. The preliminary results seem to be encouraging and show that the QMD is a very promising approach to be used in medium energy nuclear data calculation and evaluation.

We made the calculations for 20–1000 MeV neutron induced reactions by using the relativistic microscopic optical potential and obtained a global neutron relativistic phenomenological optical potential based on the available experimental data for the same energy region. The calculated cross sections and angular distributions obtained with these two kinds of potentials agree with the experimental data pretty well. These results are useful for future studies of medium energy nuclear reactions.

Based on the Letaw and Pearlstein systematic formulae and considering as many experimental data as possible, new systematic formulae for medium energy proton nonelastic and neutron total cross sections, which are in pretty good agreement with experiments for $A = 12–238$ nuclei, were obtained. Therefore, they are universal and can be used in medium energy nuclear data evaluation.

References

[1] M. Blann, CODE ALICE / 85 / 300, LLNL, UCID 20169.

[2] S. Pearlstein, J. Astrophys., 346(1989)1049.

[3] P. G. Young and E. D. Arthur, GNASH: A Preequilibrium Statistical Nuclear Model Code for Calculation of Cross–Sections Emission Spectra, Los Alamos National Laboratory, LA–6947(1977).

[4] E. D. Arthur, M. Bozoian, D. G. Madland, R. T. Perry, W. B. Wilson, and P. G. Young, Nuclear Theory for Fast Neutron Nuclear Data Evaluation, Proc. Advisory Group Meeting, Beijing, 12–16 October, 1987, IAEA–TECDOC–483, p.278 .

[5] H. W. Bertini, Phys. Rev., 188(1969)1711.

[6] HETC, Code Package CCC–178, ORNL–4744, Radiation Shielding Center, Oak Ridge National Laboratory (1977).

[7] J. Aichelin and H. Stöcker, Phys. Lett., B176(1986)14.
[8] A. Bohnet, N. Ohtsuka, J. Aichelin, R. Linden, and A. Faessler, Nucl. Phys., A494(1989)349.
[9] Li Zhuxia and Zhuo Yizhong, Comm. Nuclear Data Progress, No.5(1991)37, INDC(CPR)–021.
[10] H. W. Bertini, Phys. Rev., C6(1972)631.
[11] Shen Qing–biao, Feng Da–chun, and Zhuo Yi–zhong, Intermediate Energy Nuclear Data for Applications, Proc. Advisory Group Meeting, Vienna, 9–12 October, 1990, INDC(NDS)–245, p.129.
[12] Shen Qing–biao, Feng Da–chun, and Zhuo Yi–zhong, Phys. Rev. C43(1991)2773.
[13] Qing–biao SHEN, INDC(CPR)–020, 1991.
[14] V. McLane, C. L. Dunford, and P. F. Rose, Neutron Cross Sections, BNL–325, Vol. 2, Academic Press, 1988.
[15] S. Cierjacke, Y. Hino, et al., Phys. Rev., C36(1987)1976.
[16] D. Filges, P. Cloth and T. W. Armstrony, S. Cierjacks, Y.Hino, F.Raupp, and L. Buth, Phys. Rev., C36(1987)1988.
[17] L. G. Arnold and B. C. Clark, Phys. lett. 84B(1979)46.
[18] L. G. Arnold, B. C. Clark, and R. L. Mercer, Phys. Rev. C19(1979)917.
[19] S. Hama ,B. C. Clark, E. D. Cooper, H. S. Sherif, and R. L. Mercer, Phys. Rev. C41(1990)2737.
[20] C. J. Horowitz and B. D. Serot, Nucl. Phys. A399(1983)529.
[21] C. J. Horowitz, Nucl. Phys. A412(1984)228.
[22] Ma Zhong–yu, Zhu Ping, Gu Ying–qi, and Zhuo Yi–zhong, Nucl. Phys. A490(1988)619.
[23] J. Franz, H. P. Grotz, L. Lehmann, E. Rossle, H. Schmitt, and L. Schmitt, Nucl. Phys. A490(1988)667.
[24] S. Pearlstein, Nuclear Data for Science and Technology, proc. Inter. conf.,1988, Mito, Japan, p.1115.
[25] R. L. Schutt, R. E. Shamu, P. W. Lisowski, M. S. Moore, and G. L. Morgan, Phys. Lett. B203(1988)22.
[26] J. S. Petler M. S. Islam, R. W. Finlay, and F. S. Dietrich, Phys. Rev. C32(1985)673.
[27] J. P. Delaroche, M. S. Islam, and R. W. Finlay, Phys. Rev. C33(1986)1826.
[28] N. Olsson, B. Trostell, E. Ramstrom, and B. Holmqvist, Nuclear Data for Basic and Applied Science, Proc. Inter. Conf., Santa Fe, New Mexico, USA, 1985, p963.
[29] S. Mellema, R. W. Finlay, F. S. Dietrich, and F. Petrovich, Phys. Rev. C28(1983)2267.

[30] C. H. Johnson, D. J. Horen, and C. Mahaux, Phys. Rev. C36(1987)2252.
[31] R. L. Walter and P. P. Guss, Nuclear Data for Basic and Applied Science, Proc. Inter. Conf., Santa Fe, New Mexico, USA, 1985, p.1079.
[32] G. L. Salmon, Nucl. Phys. 21(1960)15.
[33] R. S. Harding, Phys. Rev. 111(1958)1164.
[34] J. W. Negele, Phys. Rev. C1(1970)1260.
[35] H. F. Ehrenberg, R. Hofstadter, U. Meyer–Berkhout, D. G. Ravenhall, and S. E. Sobottka, Phys. Rev. 113(1959)666.
[36] W. Bauhoff, Atom. Data and Nucl. Data Tables, 35(1986)429.
[37] R. H. McCamis, N. E. Davison, W. T. H. van Oers, R. F. Carlson, and A. J. Cox, Can. J. Phys. 64(1986)685.
[38] T. Fukahori and S. Pearlstein, Presented at IAEA Advisory Group Meeting on Intermediate Energy Nuclear Data for Applications, Vienna, Austria, 9–12, October, 1990, p.93.
[39] J. L. Letaw, R. Silberberg, and C. H. Tsao, Astrophys. J. Suppl. Ser., 51(1983)271.

Reproduced by the IAEA in Austria

October 1992